DOI: 10.1002/aenm.201401814
Article type: Communication

Disordered Lithium-Rich Oxyfluoride as Stable Host for Enhanced Li^+ Intercalation Storage

Ruiyong Chen, Shuhua Ren, Michael Knapp, Di Wang, Raiker Witter, Maximilian Fichtner, and Horst Hahn*

Dr. R. Chen, Dr. M. Knapp, Prof. M. Fichtner, Prof. H. Hahn
Helmholtz Institute Ulm, 89081 Ulm, Germany
E-mail: ruiyong.chen@kit.edu
Dr. R. Chen, Dr. S. Ren, Dr. D. Wang, Dr. R. Witter, Prof. M. Fichtner, Prof. H. Hahn
Institute of Nanotechnology, Karlsruhe Institute of Technology
P.O. Box 3640, 76021 Karlsruhe, Germany
Dr. M. Knapp
Institute for Applied Materials, Karlsruhe Institute of Technology
P.O. Box 3640, 76021 Karlsruhe, Germany
Dr. R. Witter
Technomedicum, Tallinn University of Technology
19086 Tallinn, Estonia
Prof. H. Hahn
Joint Research Laboratory Nanomaterials, Technische Universität Darmstadt
64287 Darmstadt, Germany

Keywords: Li-ion batteries, intercalation cathodes, disordered rock salt, Li_2VO_2F

Advanced cathode materials with superior energy storage capability are highly demanded for mobile and stationary applications. The inherent structural feature of Li^+ hosts is critical for the battery performance. High-capacity conversion cathode materials often encounter large voltage hysteresis (low energy efficiency) accompanied with the structural reconstruction.[1] The current commercial cathode materials are still dominated by intercalation materials with intrinsic structural integrity for accommodating Li^+.[2] However, the known intercalation materials have limited theoretical capacity (< 300 mAh g^{-1}).[3] In addition, structural transition/degradation have often been observed for the common intercalation hosts with ordered Li^+/ transition metal (TM) lattice sites. Antisite disorder (Li^+ sites/layers occupied by TM ions) in olivines can block the one-dimensional Li^+ diffusion path.[4] The activation barrier for Li^+ diffusion in layered oxides is sensitive to the Li-content, the spacing of the

oxygen layers and the interlayer cationic disorder.[5] Cationic relocation[6] and irreversible order-disorder transitions[7,8] often occur in layered oxides upon cycling. The near complete Li^+ extraction from the ordered sites/layers is concomitant with a large lattice volume change,[2] phase transition[9] and even crystal structure collapse.[10] It is desirable to develop new intercalation materials with better structural tolerance for Li^+ uptake/release and meanwhile enhanced lithium storage capability. Disordered rock-salt structures, with Li^+/TM evenly sharing cation sites and close-packed anion arrays, may be a reasonable alternative for efficient Li^+ storage. After Li^+ extraction, the TM may remain at the cation sublattice sites and uphold well the disordered rock-salt framework. A recent work based on ab initio computations revealed that Li^+ transport can be facile in a disordered cubic rock-salt oxide ($Li_{1.211}Mo_{0.467}Cr_{0.3}O_2$) with Li-excess.[8] It was found that such framework is stable with a maximum of 45% of the cation sites vacant. Herein, we demonstrate that a new dilithium disordered rock-salt Li_2VO_2F intercalation material can deliver up to about 1.8 Li^+ capacity per TM (420 mAh g^{-1}) at ~2.5 V (1000 Wh kg^{-1}) with only minor lattice volume change (~3%). Such material with mixed O^{2-}/F^- anion environment has been synthesized by a simple ball-milling method. The two Li^+ storage with V^{3+}/V^{5+} redox reactions ($Li_2VO_2F \leftrightarrow 2\ Li^+ + 2e^- + VO_2F$) leads to an attractively high theoretical capacity of 462 mAh g^{-1}. Moreover, Li_2VO_2F shows good capacity retention and minor increase in polarization upon fast charging/discharging or upon low-temperature operation.

The crystal structure of the target phase for the as-milled Li_2VO_2F is determined by Rietveld structural refinement of powder neutron (**Figure 1**a) and X-ray (Figure 1b) diffraction patterns. The refinement precludes a layered rock-salt structure (*R*-3*m* space group) (Figure S1).[11] Instead, the diffraction patterns can be well indexed in a disordered cubic rock-salt phase (space group *Fm*-3*m*, Table S1). The atomic displacement parameters were constrained to the same for all atoms in the course of the refinements. As illustrated in the inset of Figure 1a, Li and V atoms distribute randomly on the cationic sublattice (4*a*

Wyckoff sites) with a refined occupancy ratio of 0.64:0.36. The accurate occupancy refinements for O and F on the anionic sublattice (4*b* sites) cannot be obtained from the diffraction data because O and F have low contrast in scattering properties for X-rays and neutrons.[12] On average, cations are coordinated with four O and two F atoms to form the $(Li/V)O_4F_2$ octahedral units in the stoichiometric Li_2VO_2F. In addition, the refinement yields a material density of 4.25 g cm^{-3} as compared with 5 g cm^{-3} for $LiCoO_2$ and 3.5 g cm^{-3} for $LiFePO_4$.[13]

High-resolution transmission electron microscopy (HR-TEM) image shows the nanocrystalline character (~10 nm) of the as-synthesized Li_2VO_2F (Figure 1c). The cubic structure of Li_2VO_2F was also confirmed by the corresponding fast Fourier transform (FFT) image (inset in Figure 1c). Some nanocrystals (marked with white circle in Figure 1c) show clear stacking faults, arising probably from the local distortion of $(Li/V)O_xF_y$ octahedra. Energy-dispersive spectroscopy (EDS, Figure 1d) shows the identified atoms of V, F and O. The Li/V atomic ratio (~2:1) in the as-prepared material was determined by inductively coupled plasma (ICP) spectroscopy (Table S2). Certain unreacted amorphous LiF has been found from NMR. The amount of F was further semi-quantified by fluoride ion-selective electrode method and the F/V atomic ratio is about 1:1 (Table S2). Further surface and bulk chemical identification of F is shown in Figure S2.

Figure 2a shows the voltage profiles of Li_2VO_2F versus lithium measured at 40°C and C/60. The charge/discharge curves are characterized by sloping profiles and low voltage hysteresis, suggesting a single-phase intercalation process. Li_2VO_2F delivers a first discharge capacity of about 420 mAh g^{-1} and a second charge capacity of about 400 mAh g^{-1}. Further structural characterization reveals that the observed high discharge capacity upon cycling down to 1.3 V is associated to the continuous lattice volume expansion (i.e., Li^+ intercalation). Thus, approximately 1.8 Li^+ per TM cation (1080 Wh kg^{-1} and 4600 Wh L^{-1}) can be cycled for Li_2VO_2F at an average discharge voltage of 2.5 V at a slow current rate of C/60. This

indicates that about 90% of the theoretical capacity (462 mAh g^{-1}) is accessible, assuming $2Li^+$ are mobile involving the V^{3+}/V^{5+} redox couple. Such high capacity has not been observed in any intercalation-based material so far. In comparison with the classic cathode materials such as $LiFePO_4$,[14] $LiCoO_2$[15] and $LiNi_{0.5}Mn_{1.5}O_4$,[16] the discovered new intercalation material Li_2VO_2F exhibits a substantial increase in capacity. Li_2VO_2F also shows good capacity retention when increasing current rates from C/60 to C/5 (345 mAh g^{-1}) and 1C (300 mAh g^{-1}, 3100 Wh L^{-1}) (Figure 2b). Only a slight increase (~0.11 V) in the overpotential was observed when increasing the C-rates (Figure 2c). Figure 2d shows the capacity retention percentages at different C-rates. Better capacity retention was observed when higher C-rates were applied. The observed capacity decay may arise from the electrode material/electrolyte interactions, rather than from the structural degradation of Li_2VO_2F.

The conductivity of the Li_2VO_2F was measured by *ac* impedance spectroscopy at various temperatures (Figure S3). The activation energy (E_a) was calculated to be 0.18 eV from the slope of the $\log(\sigma T)$ versus T^{-1} plot by the Arrhenius equation, where σ is conductivity and T is temperature (Figure 2e). This value is lower than that of $LiFePO_4$ (about 0.2–0.6 eV).[17] The room temperature conductivity of Li_2VO_2F is about 2.2×10^{-7} S cm^{-1}, which is two orders of magnitude higher than that of $LiFePO_4$.[17] As concluded from a recent work,[8] in a disordered rock-salt oxide having Li in excess, the energy barrier for Li^+ hopping from one octahedral site to a neighbor octahedral site can be reduced to an applicable level (~0.3 eV). The high Li/V ratio (2:1) in the present cation/anion-disordered Li_2VO_2F lattice is expected to enable an active percolating network for Li^+ diffusion. These transport properties hint at fast intrinsic kinetics of Li_2VO_2F. Furthermore, cyclic voltammetry (CV) experiments were performed for the nanosized Li_2VO_2F with varied scan rates (0.02–5 mV s^{-1}) (**Figure 3**a,b). The cathodic peak current response (i_c) is proportional to the square root of scan rate ($v^{0.5}$) (Figure 3b), revealing that the Li^+ storage arises mainly from a solid-state diffusion-controlled intercalation mechanism rather than pseudocapacitive response.[18]

Detailed crystal and electronic structure changes of the Li_2VO_2F upon cycling were investigated (**Figure 4**a-c**)**. A continuous and reversible diffraction peak shift (Figure 4a) and lattice constant change (Figure 4b) was observed on charge/discharge, implying the reversibility of the single-phase insertion-extraction process. The lattice volume shrinks by 3.3% after Li^+ extraction (with 60% of the disordered cation sites vacant), compared with 6.8% for $LiFePO_4$.[14,19] The TEM image and electron diffraction pattern for the charged sample confirms that the cubic rock-salt domain structure maintains (inset in Figure 4c, Figure S4). At the end of the discharge (Figure S5), there was no evidence of any new phase or additional Li^+ occupancy at the tetrahedral 8*c* sites (different from the observation for a layered $Li_{1.07}V_{0.93}O_2$[11]). A slight increase (+0.64%) in the lattice volume was observed for the discharged sample (69.83 $Å^3$) in comparison with that of the as-prepared sample, indicating that certain additional Li^+ were inserted into the crystal lattice after one charge/discharge cycle. A very weak electron paramagnetic resonance (EPR) signal was detected for the as-prepared sample (Figure S6), suggesting the existence of certain V^{4+} in the as-prepared material. Note that V^{3+} ions (non-Kramer's ions) are silent under general EPR experimental conditions, whereas V^{4+} has a strong EPR resonance signal.[20] These results may suggest an off-stoichiometric $Li_{2-x}VO_2F$ starting composition. Such off-stoichiometric composition may explain the slightly low first charge capacity as observed in Figure 2a. Further excess of the lithium source in the material synthesis might be necessary to balance the first charge and discharge capacities.

Energy-loss near edge structure (ELNES) spectra of the pristine Li_2VO_2F in Figure 4c show well separated V L_3 (518 eV) and L_2-edges (524.2 eV) owning to the V 2p-3d dipole transition.[21] The O K-edge (541.8 eV) and O pre-edge (533 eV) are characteristics of hybridization between O(2p)-V(4sp) and O(2p)-V(3d), respectively.[22] On charging to 4.1 V, the V L-edges shifted by about 1 eV to higher energy loss (with a maximum of 519 eV for the V L_3-edge, typical for V^{5+})[23] and the L_3/L_2 white line ratio was reduced. These changes

evidenced the oxidation of V with the extraction of Li^+.[24] For the charged sample the ELNES spectra taken at different lateral positions show slight difference (Figure 4c), which may arise from an inhomogeneous mixing of Li_2VO_2F nanoparticles with carbon black. Delithiation leads to substantial changes in the O chemical bonding, as revealed from the O K-edge ELNES spectra (Figure 4c). The O pre-edge peak shifted to lower energy loss indicating enhanced O(2p)–V(3d) hybridization,[22] with an increased intensity (charge compensation effect as lithium is extracted)[25] and the main peak shifted to higher energy loss with a decreased intensity. The presence of two O pre-edge peaks may be attributed to the formation of mixed vanadium oxidation states (mixed hybridized states). These observations suggest the change of local symmetry of oxygen atoms, nearby coordination and its hybridization with neighboring V atoms in the delithiated sample.[21] After discharging to 1.3 V, the V and O ELNES profiles are quite similar to that for the pristine material (data now shown), indicating reversible change in electronic structures.

^{7}Li and ^{19}F MAS NMR measurements were performed to probe the Li and F environments in pristine Li_2VO_2F and their involvement in the electrochemical cycling (Figure 4d,e). As expected, the ^{7}Li (-9.1 ppm) and ^{19}F NMR (-201 and -205 ppm) spectra are characterized by broad resonance lines in the pristine material, due to the large distribution of chemical shifts in the disordered rock-salt structure. The sharp ^{7}Li NMR (~0 ppm) and ^{19}F (-204.8 ppm) signals arises from residual diamagnetic LiF precursor (not found from diffraction data).[26] Two broad ^{19}F resonance lines were observed, indicating that F exists in two distinct environments arising from (i) non-uniform distribution of F at surface and in the bulk as evidenced from X-ray photoelectron spectroscopy (XPS) and EDS analysis (Table S2), and (ii) local crystal lattice distortion as observed in TEM. The difference in the width of the ^{19}F resonance lines is related to the local symmetric environments. These ^{7}Li and ^{19}F NMR lines show positive shifts after charging to 4.1 V and then shift back after discharging to 1.3 V (Figure 4d,e, Table S3), which is related to the redox of V and a largely reversible structural

change. Additional ^{19}F lines at ~153 ppm were observed (indicated by arrows in Figure 4e) in the cycled samples for unclear reasons (Note that LiBOB was used as electrolyte for collecting ^{19}F NMR samples, Figure S7). When Li^+ ions are extracted from the lattice, a Li-vacancy reordering may occur to relieve the electrostatic repulsion, and to minimize the delithiation-induced lattice strain and volume change. This may also result in a decrease in symmetry. ^{51}V MAS NMR was also recorded tentatively (Figure 4f). The ^{51}V NMR signal is invisible for the discharged sample, which suggests that only V^{3+} paramagnetic ions exist. The observed ^{51}V NMR signal for the as-prepared sample may arise from certain V^{4+} ions, as identified from the EPR experiments.

Figure 5a-d shows the temperature-dependent electrochemical performance for the Li_2VO_2F/Li half-cells. At 25°C, a reversible discharge capacity of about 330 and 320 mAh g^{-1} was observed at C/60 and C/20, respectively. At -10°C, Li_2VO_2F can still deliver a high reversible discharge capacity of about 280 and 240 mAh g^{-1} at C/60 and C/20, respectively. These results confirm good capacity retention and cyclability of Li_2VO_2F at low temperatures. Furthermore, no noticeable increase in polarization can be observed by decreasing the cycling temperature from 40°C to 25°C and to -10°C (lithiation voltage at ~2.42 V, inset in Figure 5d). These results confirmed again a fast kinetic behavior for the Li_2VO_2F. In contrast, by decreasing the temperature from 25°C to -10°C, $LiFePO_4$[27] and $LiNi_{1/3}Mn_{1/3}Co_{1/3}O_2$[28] cathode materials showed relatively large increase in polarization with a discharge voltage shifted down by ~0.3 V.

The full-cell performance using Li_2VO_2F as cathode and graphite as anode was studied. The graphite electrode was firstly discharged to 0.01 V and then charged to 2 V against lithium. The charged graphite electrode was reassembled against Li_2VO_2F cathode. Figure 5e shows the Li_2VO_2F/graphite full-cell voltage profiles at 25°C and C/20. A reversible capacity of about 320 mAh g^{-1} was observed at a discharge voltage of ~2.5 V. This value is close to

that for the Li_2VO_2F/Li half-cell measured at the same current rate and temperature. Accordingly, an overall energy density of about 800 Wh kg^{-1} was obtained for Li_2VO_2F/graphite full-cell. Such energy density is slightly higher than that (about 740 Wh kg^{-1}) for the $Li_{1.2}Ni_{0.15}Mn_{0.55}Co_{0.1}O_2$/graphite full-cell cycled between 2 and 4.6 V at 30°C and about 4.65 mA g^{-1}.[29] These preliminary results confirm that a high reversible capacity/energy-density can be still obtained for the Li_2VO_2F when using a Li-free anode.

In conclusion, we demonstrate for the first time a new intercalation material Li_2VO_2F with a disordered rock-salt structure enabling up to about 1.8 Li^+ intercalation capacity per TM cation. The crystal framework maintains well leaving 60% of the cation sites vacant with a lattice volume change of only ~3%. Moreover, the disordered rock-salt host structure also allows fast Li^+ transport with good *ac* electronic conductivity. A high capacity of 300 mAh g^{-1} is accessible at 1C rate at 40°C. From 25°C to -10°C, Li_2VO_2F exhibits good capacity retention. Interestingly, there is no increase in the polarization for the Li_2VO_2F when decreasing the experimental temperature from 40°C to -10°C. When evaluated at full-cell using graphite as anode, Li_2VO_2F/graphite shows comparable cell capacity and cell voltage in comparison with the Li_2VO_2F/Li half-cell. These properties for Li_2VO_2F are suggestive for developing new structure-stable and high-capacity energy-storage materials with better combination of mixed cation/anion in a disordered rock salt structure.

Supporting Information
Supporting Information is available from the Wiley Online Library or from the author.

Acknowledgements
We thank E. Maawad, O. Dolotko, A. Senyshyn (Neutron diffraction), V. Trouillet (XPS) and T. Bergfeldt (ICP) for sample measurements. R.W. thanks the EU Fund, Estonian Research Council, TUT and KBFI (MTT68, SF0690034s09, B618 and PUT126).

Received: ((will be filled in by the editorial staff))
Revised: ((will be filled in by the editorial staff))
Published online: ((will be filled in by the editorial staff))

[1] a) P. G. Bruce, S. A. Freunberger, L. J. Hardwick, J.-M. Tarascon, *Nature Mater.* **2012**, *11*, 19; b) F. Badway, F. Cosandey, N. Pereira, G. G. Amatucci, *J. Electrochem. Soc.* **2003**, *150*, A1318.

[2] M. S. Whittingham, *Chem. Rev.* **2004**, *104*, 4271.

[3] a) M. M. Thackeray, C. S. Johnson, J. T. Vaughey, N. Li, S. A. Hackney, *J. Mater. Chem.* **2005**, *15*, 2257; b) N. Yabuuchi, K. Yoshii, S.-T. Myung, I. Nakai, S. Komaba, *J. Am. Chem. Soc.* **2011**, *133*, 4404; c) C. Masquelier, L. Croguennec, *Chem. Rev.* **2013**, *113*, 6552; d) M. M. Thackeray, W. I. F. David, P. G. Bruce, J. B. Goodenough, *Mater. Res. Bull.* **1983**, *18*, 461.

[4] S. Adams, *J. Solid State Electrochem.* **2010**, *14*, 1787.

[5] a) K. Kang, G. Ceder, *Phys. Rev. B* **2006**, *74*, 094105; b) K. Kang, Y. S. Meng, J. Bréger, C. P. Grey, G. Ceder, *Science* **2006**, *311*, 977.

[6] a) A. C. W. P. James, J. B. Goodenough, *J. Solid State Chem.* **1988**, *76*, 87; b) Q. D. Truong, M. K. Devaraju, Y. Sasaki, H. Hyodo, T. Tomai, I. Honma, *Chem. Mater.* **2014**, *26*, 2770; c) M. Wagemaker, F. G. B. Ooms, E. M. Kelder, J. Schoonman, G. J. Kearley, F. M. Mulder, *J. Am. Chem. Soc.* **2004**, *126*, 13526.

[7] a) J. N. Reimers, J. R. Dahn, *J. Electrochem. Soc.* **1992**, *139*, 2091; b) C. Delmas, H. Cognac-Auradou, J. M. Cocciantelli, M. Ménétrier, J. P. Doumerc, *Solid State Ionics* **1994**, *69*, 257.

[8] a) J. Lee, A. Urban, X. Li, D. Su, G. Hautier, G. Ceder, *Science* **2014**, *343*, 519; b) A. Urban, J. Lee, G. Ceder, *Adv. Energy Mater.* **2014**, *4*, 1400478.

[9] a) G. G. Amatucci, J. M. Tarascon, L. C. Klein, *J. Electrochem. Soc.* **1996**, *143*, 1114; b) A. Van der Ven, M. K. Aydinol, G. Ceder, *J. Electrochem. Soc.* **1998**, *145*, 2149; c) R. Chen, M. Knapp, M. Yavuz, R. Heinzmann, D. Wang, S. Ren, V. Trouillet, S. Lebedkin, S. Doyle, H. Hahn, H. Ehrenberg, S. Indris, *J. Phys. Chem. C* **2014**, *118*, 12608.

[10] a) H. Lee, S.-D. Park, J. Moon, H. Lee, K. Cho, M. Cho, S. Y. Kim, *Chem. Mater.* **2014**, *26*, 3896; b) R. Chen, R. Heinzmann, S. Mangold, V. S. K. Chakravadhanula, H. Hahn, S. Indris, *J. Phys. Chem. C* **2013**, *117*, 884.

[11] A. R. Armstrong, C. Lyness, P. M. Panchmatia, M. S. Islam, P. G. Bruce, *Nature Mater.* **2011**, *10*, 223.

[12] V. F. Sears, *Neutron News* **1992**, *3*, 26.

[13] S.-Y. Chung, J. T. Bloking, Y.-M. Chiang, *Nature Mater.* **2002**, *1*, 123.

[14] A. K. Padhi, K. S. Nanjundaswamy, J. B. Goodenough, *J. Electrochem. Soc.* **1997**, *144*, 1188.

[15] a) K. Mizushima, P. C. Jones, P. J. Wiseman, J. B. Goodenough, *Mater. Res. Bull.* **1980**, *15*, 783; b) J. Cho, Y. J. Kim, B. Park, *Chem. Mater.* **2000**, *12*, 3788.

[16] a) Q. Zhong, A. Bonakdarpour, M. Zhang, Y. Gao, J. R. Dahn, *J. Electrochem. Soc.* **1997**, *144*, 205; b) A. Manthiram, K. Chemelewski, E.-S. Lee, *Energy Environ. Sci.* **2014**, *7*, 1339.

[17] a) C. Delacourt, L. Laffont, R. Bouchet, C. Wurm, J.-B. Leriche, M. Morcrette, J.-M. Tarascon, C. Masquelier, *J. Electrochem. Soc.* **2005**, *152*, A913; b) R. Malik, A. Abdellahi, G. Ceder, *J. Electrochem. Soc.* **2013**, *160*, A3179.

[18] V. Augustyn, J. Come, M. A. Lowe, J. W. Kim, P.-L. Taberna, S. H. Tolbert, H. D. Abruña, P. Simon, B. Dunn, *Nature Mater.* **2013**, *12*, 518.

[19] A. S. Andersson, B. Kalska, L. Häggström, J. O. Thomas, *Solid State Ionics* **2000**, *130*, 41.

[20] C. P. Poole, H. A. Farach, *The Theory of Magnetic Resonance*. Wiley-Interscience, New York, **1972**.

[21] F. M. F. de Groot, M. Grioni, J. C. Fuggle, J. Ghijsen, G. A. Sawatzky, H. Petersen, *Phys. Rev. B* **1989**, *40*, 5715.

[22] a)W.-S. Yoon, K.-B. Kim, M.-G. Kim, M.-K. Lee, H.-J. Shin, J.-M. Lee, J.-S. Lee, C.-H. Yo, *J. Phys. Chem. B* **2002**, *106*, 2526; b) S. Hwang, W. Chang, S. M. Kim, D. Su, D. H. Kim, J. Y. Lee, K. Y. Chung, E. A. Stach, *Chem. Mater.* **2014**, *26*, 1084.

[23] J. G. Chen, C. M. Kim, B. Frühberger, B. D. de Vries, M. S. Touvelle, *Sur. Sci.* **1994**, *321*, 145.

[24] X. W. Lin, Y. Y. Wang, V. P. Dravid, P. M. Michalakos, M. C. Kung, *Phys. Rev. B* **1993**, *47*, 3477.

[25] a) G. Ceder, Y.-M. Chiang, D. R. Sadoway, M. K. Aydinol, Y.-I. Jang, B. Huang, *Nature* **1998**, *392*, 694; b) J. Graetz, C. C. Ahn, R. Yazami, B. Fultz, *J. Phys. Chem. B* **2003**, *107*, 2887; c) M. K. Aydinol, A. F. Kohan, G. Ceder, K. Cho, J. Joannopoulos, *Phys. Rev. B* **1997**, *56*, 1354.

[26] M. Ménétrier, J. Bains, L. Croguennec, A. Flambard, E. Bekaert, C. Jordy, Ph. Biensan, C. Delmas, *J. Solid State Chem.* **2008**, *181*, 3303.

[27] X.-L. Wu, Y.-G. Guo, J. Su, J.-W. Xiong, Y.-L. Zhang, L.-J. Wan, *Adv. Energy Mater.* **2013**, *3*, 1155.

[28] Y. Ji, Y. Zhang, C.-Y. Wang, *J. Electrochem. Soc.* **2013**, *160*, A636.

[29] Y. Li, M. Bettge, B. Polzin, Y. Zhu, M. Balasubramanian, D. P. Abraham, *J. Electrochem. Soc.* **2013**, *160*, A3006.

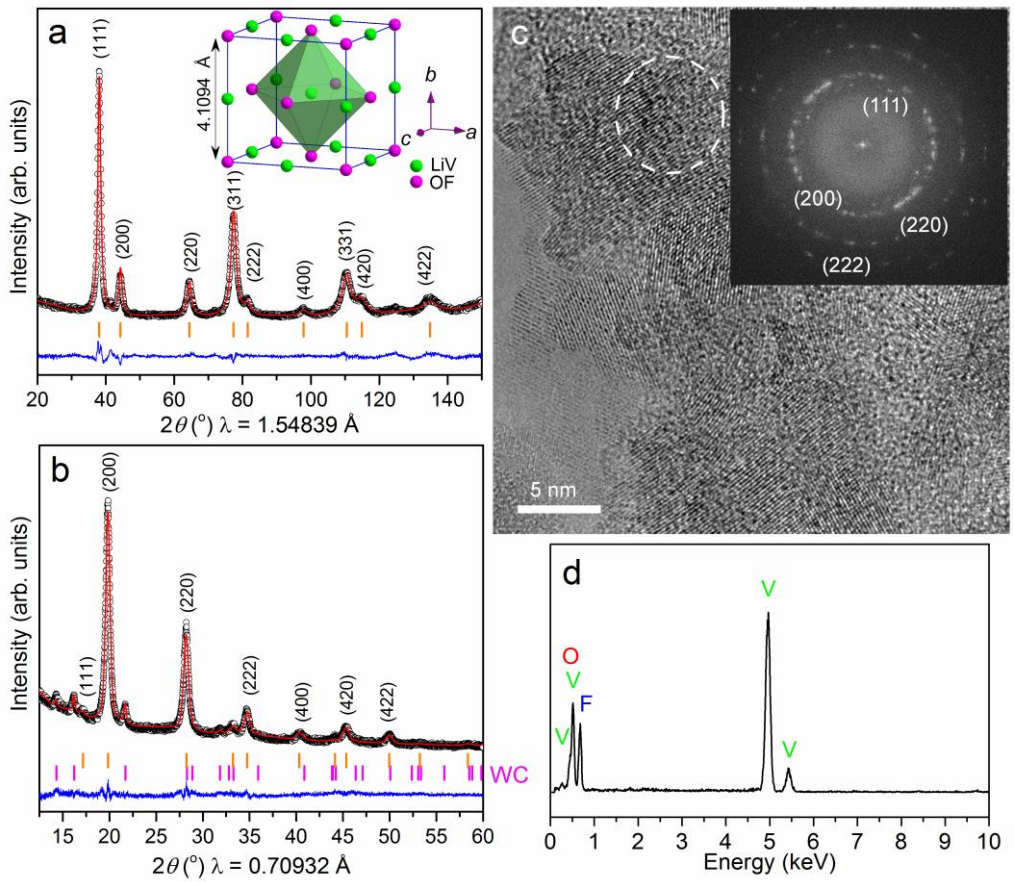

Figure 1. (a) Neutron and (b) X-ray diffraction (Mo Kα_1 radiation) patterns of Li_2VO_2F and Rietveld refinement with a cubic rock-salt phase (*Fm*-3*m* space group, a = 4.1093 Å and V = 69.39 Å^3). Inset in (a) shows the disordered rock-salt unit cell. (c) HR-TEM image and FFT pattern (inset). (d) EDS spectrum.

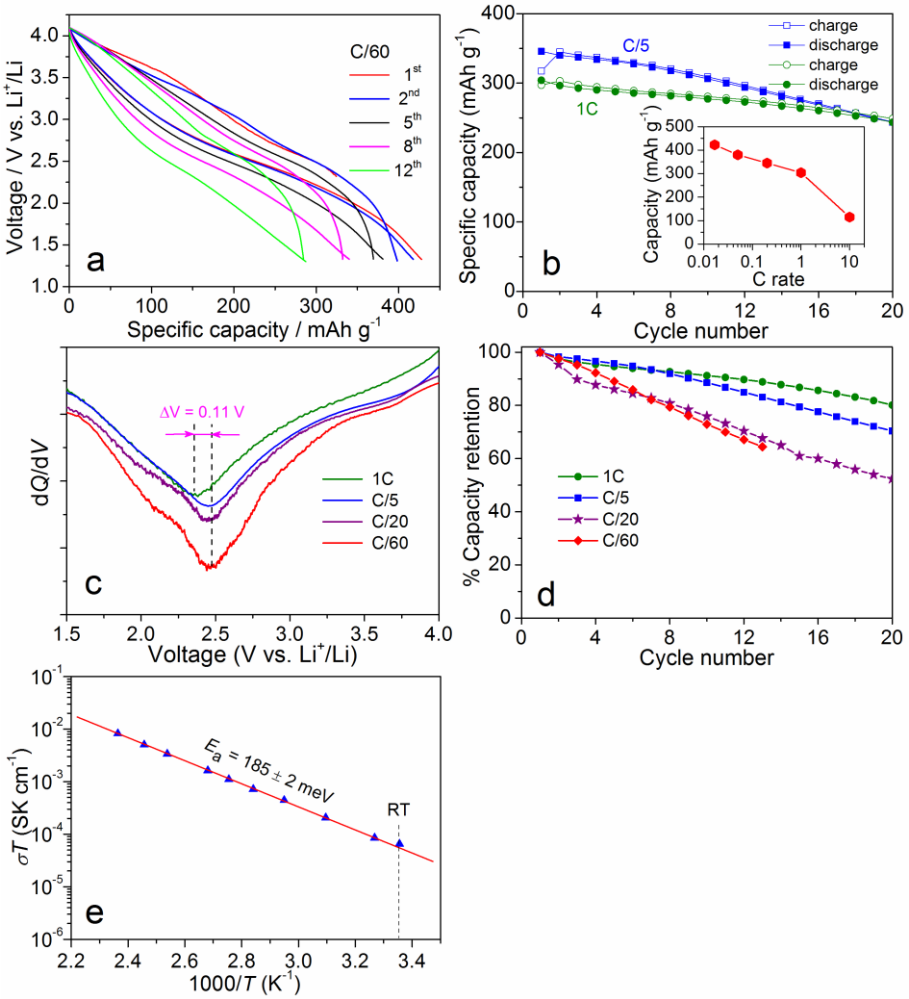

Figure 2. (a) Voltage profiles of Li_2VO_2F cycled at 40°C and C/60. (b) Cyclability at C/5 and 1C. Inset in (b) shows the capacity retention with increasing C-rates from C/60 to 10C. (c) d*Q*/d*V* profiles. (d) Capacity retention percentage as a function of applied C-rates. (e) Arrhenius plot of ac electrical conductivity of a Li_2VO_2F pellet.

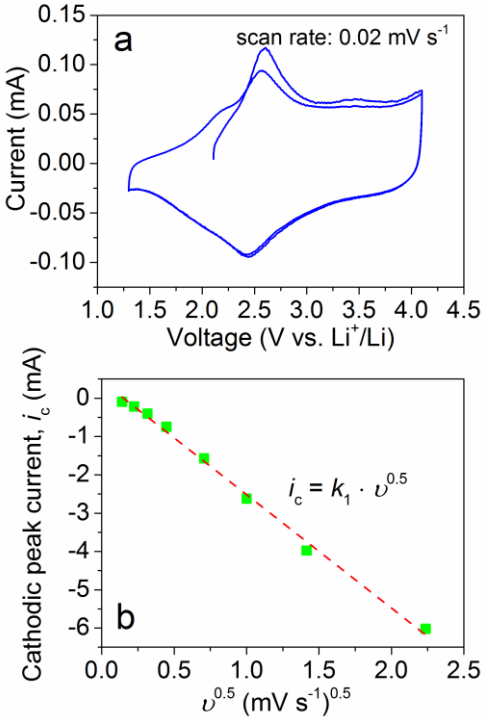

Figure 3. (a) CV curves at a scan rate of 0.02 mV s^{-1}. (b) The plot of cathodic peak current versus the square root of sweep rate.

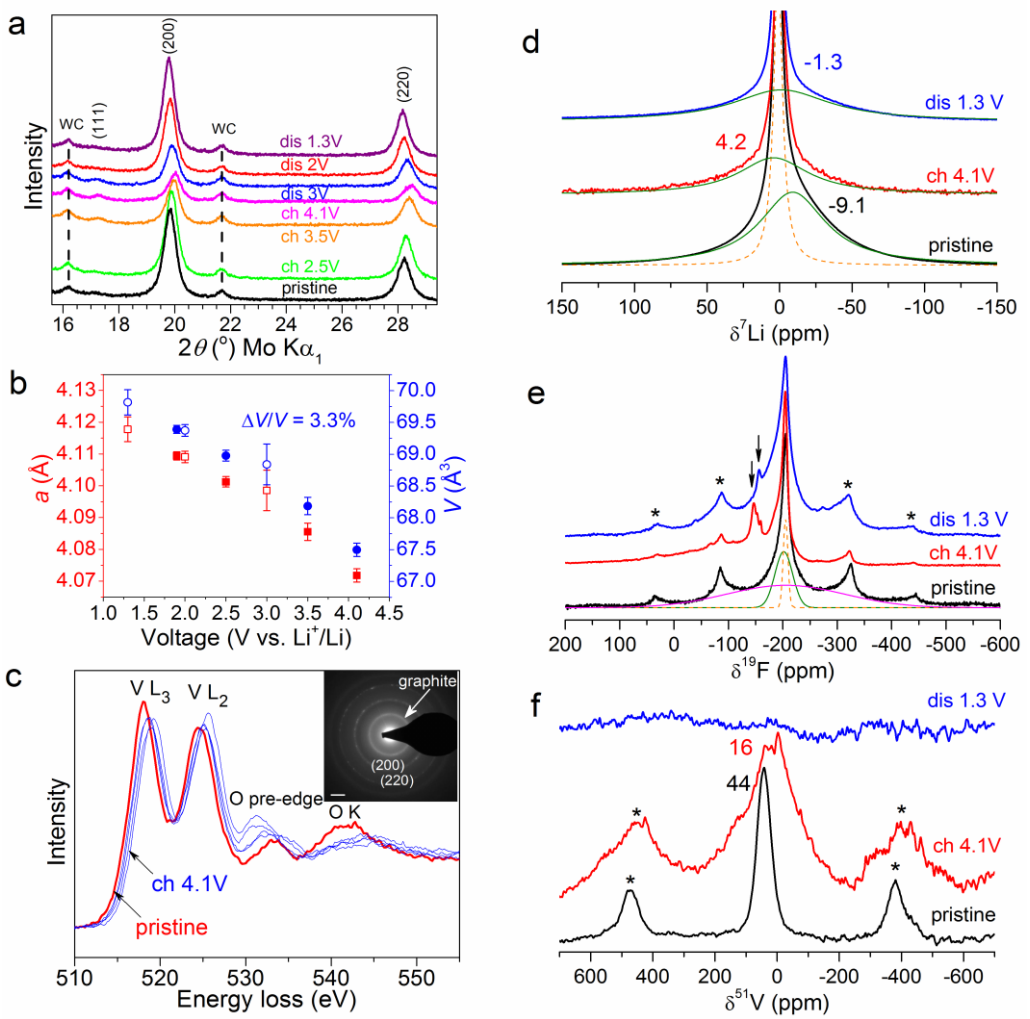

Figure 4. Structural changes of Li_2VO_2F over cycling measured at 40°C and C/60. (a) Shift of (200) and (220) diffraction peaks. (b) Changes in lattice constants, with filled and open symbols for charge and discharge, respectively. (c) ELNES of V $L_{2,3}$ and O K-edges of pristine Li_2VO_2F and sample charged to 4.1 V. Inset in (c) shows the electron diffraction pattern of charged Li_2VO_2F. Changes of (d) ^{7}Li, (e) ^{19}F and (f) ^{51}V MAS NMR spectra. The * denote the spinning sidebands.

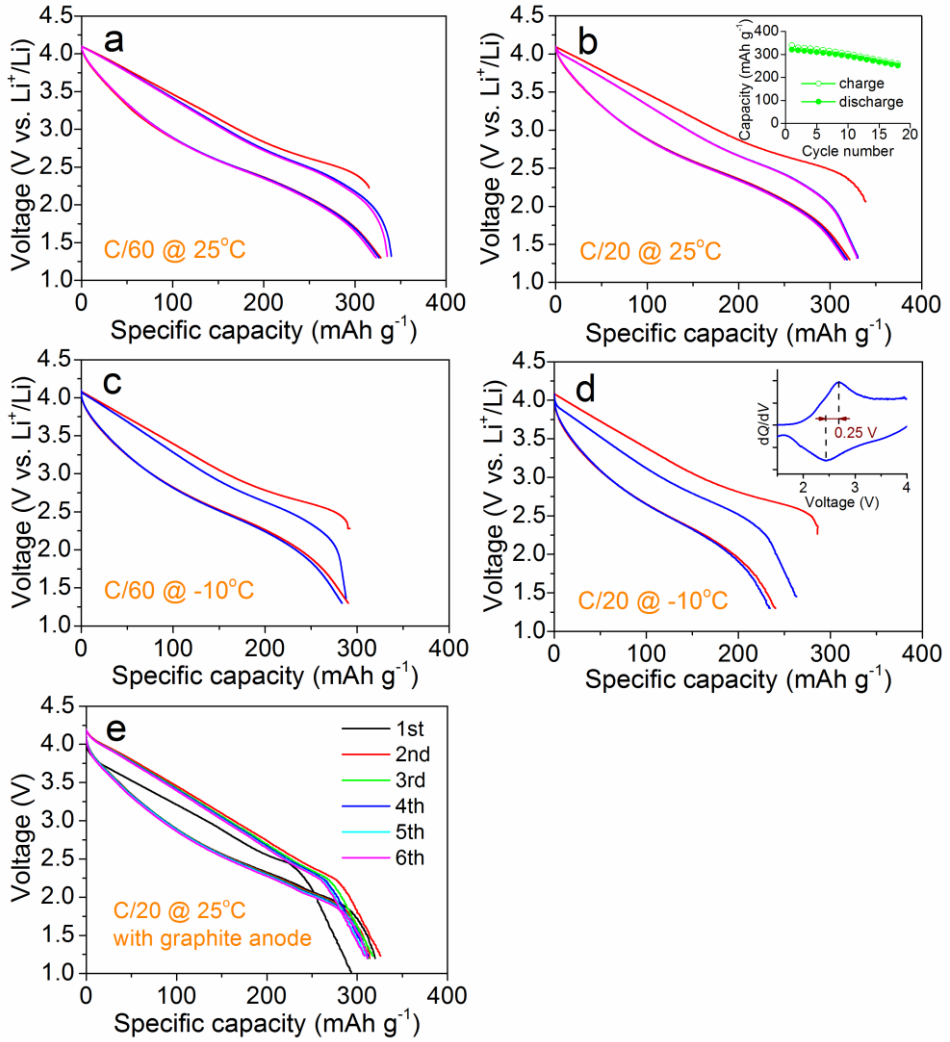

Figure 5. Voltage profile of Li_2VO_2F cycled (a,b) at 25°C and (c,d) at -10°C. Inset in (b) shows the corresponding cyclability. Inset in (d) shows the d*Q*/d*V* profile of the second cycle. (e) Voltage profiles of Li_2VO_2F/graphite full-cell measured at 25°C and C/20.

A new intercalation compound Li_2VO_2F with disordered rock salt structure enables up to about 1.8 Li^+ storage (420 mAh g^{-1}) at ~2.5V with a lattice volume change of only ~3%. A high capacity of 300 mAh g^{-1} at 1C rate is observed. At -10°C, Li_2VO_2F can deliver a reversible capacity of 280 mAh g^{-1} at ~2.4 V.

Keywords: Li-ion batteries, intercalation cathodes, disordered rock salt, Li_2VO_2F

R. Chen,* S. Ren, M. Knapp, D. Wang, R. Witter, M. Fichtner, H. Hahn

Disordered Lithium-Rich Oxyfluoride as Stable Host for Enhanced Li^+ Intercalation Storage